

# Many-body effects in iron pnictides and chalcogenides – non-local vs dynamic origin of effective masses

Jan M. Tomczak,<sup>1</sup> M. van Schilfgaarde,<sup>2</sup> and G. Kotliar<sup>1</sup>

<sup>1</sup>*Department of Physics and Astronomy, Rutgers University, Piscataway, New Jersey 08854, USA*

<sup>2</sup>*Department of Physics, Kings College London, Strand, London WC2R 2LS*

We apply the quasi-particle self-consistent  $GW$  (QSGW) approximation to some of the iron pnictide and chalcogenide superconductors. We compute Fermi surfaces and density of states, and find excellent agreement with experiment, substantially improving over standard band-structure methods. Analyzing the QSGW self-energy we discuss non-local and dynamic contributions to effective masses. We present evidence that the two contributions are mostly separable, since the quasi-particle weight is found to be essentially independent of momentum. The main effect of non locality is captured by the static but non-local QSGW effective potential. Moreover, these non-local self-energy corrections, absent in e.g. dynamical mean field theory (DMFT), can be relatively large. We show, on the other hand, that QSGW only partially accounts for dynamic renormalizations at low energies. These findings suggest that QSGW combined with DMFT will capture most of the many-body physics in the iron pnictides and chalcogenides.

PACS numbers: 74.70.Xa, 71.27.+a, 71.15.-m

The discovery of superconductivity in the iron pnictides and chalcogenides has triggered much effort into understanding their electronic properties.[1] The first theoretical insight into the pnictides was gained by density functional theory (DFT) within the local density approximation (LDA), which correctly predicted the Fermi surfaces of LaFePO[2] and LaFeAsO[3], as well as the striped antiferromagnetic spin ground state[4]. However there is ample experimental evidence for sizable correlation effects in the pnictides, manifesting themselves in high effective masses as witnessed by optical spectroscopy[5], de Haas-van Alphen measurements[6], or bandwidth renormalizations from photoemission spectroscopy (PES) [7–11], as well as low magnetic moments [12, 13]. These issues have been successfully addressed by many-body techniques, yielding correct effective masses[14, 15], ordered moments[14], and good structures[16, 17].

In many of these works, however, correlation effects have been accounted for by treating local interactions for a subspace of orbitals only. While this improves the description, several shortcomings persist : (a) correcting only a subspace means that large parts of the electronic structure are still DFT derived. The choice of the exchange-correlation functional being discretionary, moreover causes a dependence on the effective one-particle starting point. Also, results depend on the correlated subspace chosen. (b) Out-of-subspace self-energies[18] are neglected, leading e.g. to underestimates in p-d gaps. (c) Non local interactions are treated on the effective one-particle level. To address these issues, we applied the quasi-particle self-consistent  $GW$  approximation [19–21] to the iron pnictides and chalcogenides. We discuss band-structures, Fermi surfaces, and density of states (DOS) and elucidate the origin of many-body effective masses. The essence of our findings is : (1) Non-local self-energy effects are not small. These are neglected in

DMFT[22] based approaches. (2) QSGW, which includes non-local correlations, produces excellent Fermi surfaces, but (3) does not adequately account for the dynamics of the self-energy. (4) Non-locality and energy dependence are shown to be essentially separable. (5) Together, this indicates that a combined QSGW+DMFT approach is a very promising avenue in electronic structure theory.

An important goal of the many-body theory of solids is to capture the one-particle Greens-function  $G$ , which is written as  $G^{-1} = \omega - H^0(\mathbf{k}) - \Sigma(\mathbf{k}, \omega)$ , with  $H^0$  a reference one-particle Hamiltonian, and  $\Sigma$  a self-energy that is defined with respect to correlation effects already included in  $H^0$ [42]. For example, in LDA+DMFT[22],  $H^0 = H^{\text{LDA}} = -\nabla^2 + v_{\text{crystal}} + v_{\text{Hartree}} + v_{\text{xc}}^{\text{LDA}}$ , is the Kohn-Sham Hamiltonian, with  $\Sigma = (\Sigma^{\text{DMFT}}(\omega) - E_{dc})_{LL'RR'} |RL\rangle \langle R'L'|$ . The self-energy  $\Sigma^{\text{DMFT}}$  acts on a set of correlated orbitals  $|RL\rangle$ , and the portion  $E_{dc}$  of  $\Sigma^{\text{DMFT}}$  already contained in  $H^0$  must be subtracted. In the QSGW approximation,  $H^0 = H^{\text{QSGW}} = -\nabla^2 + v_{\text{crystal}} + v_{\text{Hartree}} + v_{\text{xc}}^{\text{QSGW}}$ , and  $\Sigma^{\text{QSGW}} = G^{\text{QSGW}} W - v_{\text{xc}}^{\text{QSGW}}$ , where the (static) QSGW exchange-correlation potential,  $v_{\text{xc}}^{\text{QSGW}}$ , is chosen so as to closely mimic the same quasi-particles  $E_{\mathbf{k}j}$  in  $H^{\text{QSGW}}$  as in  $(\omega - H^{\text{QSGW}} - \Sigma^{\text{QSGW}})$ . These are given by

$$[H^{\text{QSGW}}(\mathbf{k}) + \Re \Sigma^{\text{QSGW}}(\mathbf{k}, E_{\mathbf{k}j})] |\Psi_{\mathbf{k}j}\rangle = E_{\mathbf{k}j} |\Psi_{\mathbf{k}j}\rangle \quad (1)$$

and it can be shown[19] that a good choice for  $v_{\text{xc}}^{\text{QSGW}}$  is

$$\frac{1}{2} \sum_{ijk} |\Psi_{\mathbf{k}i}\rangle \Re [\Sigma_{ij}^{\text{QSGW}}(\mathbf{k}, E_{\mathbf{k}i}) + \Sigma_{ji}^{\text{QSGW}}(\mathbf{k}, E_{\mathbf{k}j})] \langle \Psi_{\mathbf{k}j} |. \quad (2)$$

Results for paramagnetic BaFe<sub>2</sub>As<sub>2</sub> are shown in Fig. 1. As is clearly visible, QSGW substantially narrows the iron 3d bands (by 16%) relative to the Kohn-Sham spectrum within LDA[43]. This narrowing corresponds to an enhancement of the effective mass,  $m^{\text{QSGW}}/m^{\text{LDA}}$ ,

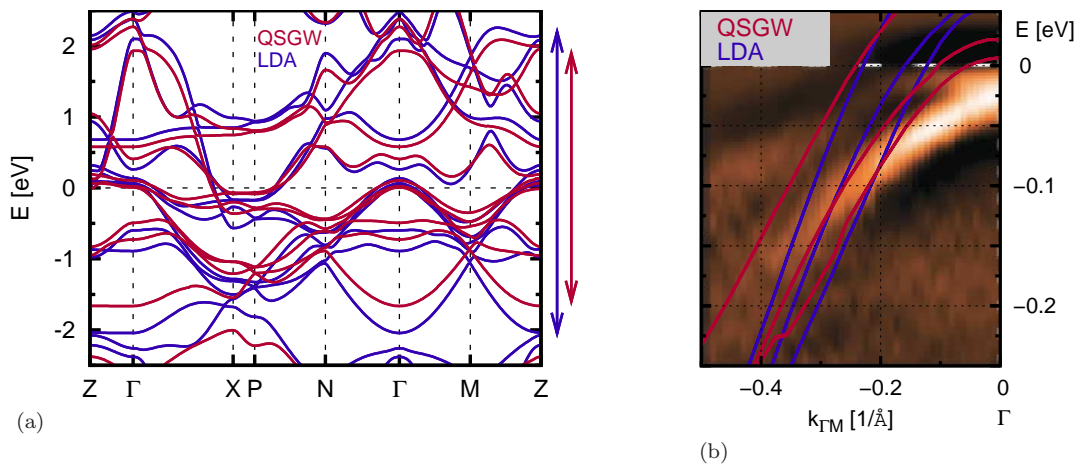


FIG. 1: **paramagnetic BaFe<sub>2</sub>As<sub>2</sub>**. (a) bandstructures within LDA and QSGW (notice the Fe-3d bandwidth narrowing as indicated by the arrows), (b) comparison with ARPES[23] around the  $\Gamma$  point. The slight constant energy shift between theory and experiment possibly originates from doping in the measured sample, BaFe<sub>1.85</sub>Co<sub>0.15</sub>As<sub>2</sub>[23].

and is slightly larger than the 12% found for elemental iron[20] (See Tab. I for other compounds). In Fig. 1(b) we compare QSGW and LDA bands near the Fermi level  $E_F$  and  $\mathbf{k}$  near zero, to angle resolved photoemission (ARPES) experiments[23]. It is consensus from experimental data that there is, at the  $\Gamma$  point, an outer hole pocket, while closer to  $\Gamma$  there are two xz/yz excitations [9, 23, 24]. The top of these inner bands is very close to zero[23], particularly for Co-doped samples[23, 25]. The character of the outer pocket is debated : a mixture of xy and  $x^2-y^2$  [23],  $z^2$  additions[26], and a change of character along  $k_z$ [26] is reported. The Fermi vector has been measured for the outer band only :  $k_F=0.07-0.17\text{\AA}^{-1}$ [23, 24, 27]. QSGW hardly effects this pocket, and it indeed is mainly of xy character for both LDA and QSGW. The Fermi wave vector is  $k_F=0.24\text{\AA}^{-1}$ . The inner pockets are of xz/yz character, in accord with experiment [23, 25]. Relative to LDA, their size is reduced to  $k_F=0.05\text{\AA}^{-1}$  and  $k_F=0.11\text{\AA}^{-1}$ [44].

While QSGW reduces the group velocity relative to LDA, the dispersion at  $k_F$  near  $\Gamma$  as measured by ARPES is still a factor of two or so smaller. This suggests that QSGW does not fully account for all many-body renormalizations in this compound, as we detail below.

We next consider the chalcogenide FeSe (Fig. 2). The QSGW band-structure displays a remarkable narrowing of the iron 3d bands of 22%, equally visible in the DOS. Also higher energy bands get renormalized : Se-4p excitations are pushed down in energy, notably improving the agreement with PES.[11] In Fig. 2(c-e) we compare the Fermi surfaces of FeSe and FeTe within QSGW and LDA with measurements of the Fe<sub>1.04</sub>Te<sub>0.66</sub>Se<sub>0.34</sub> alloy[28]. In experiment there are three hole pockets at  $\Gamma$  and two electron pockets around  $M$ . QSGW and LDA predict similar surfaces for the xy pocket labeled “ $\gamma$ ”, and the Fermi wave vectors (FeSe :  $k_F^\gamma = 0.29\text{\AA}^{-1}$ ,

FeTe :  $k_F^\gamma = 0.43\text{\AA}^{-1}$ ) encompass the ARPES value for Fe<sub>1.04</sub>Te<sub>0.66</sub>Se<sub>0.34</sub> ( $k_F^\gamma = 0.3\text{\AA}^{-1}$ ). The QSGW Fermi vectors of the xz/yz “ $\alpha$ ” and “ $\beta$ ” pockets shrink relative to the LDA, and become more anisotropic. Indeed, the “ $\alpha$ ” pocket has  $k_F^\alpha = 0.04\text{\AA}^{-1}$  on the  $\Gamma M$  line for FeSe, and completely disappears in FeTe. The magnitude agrees well with ARPES measurements ( $k_F^\alpha = 0.03\text{\AA}^{-1}$ ), whereas the ARPES  $\beta$  pocket ( $k_F^\beta = 0.12\text{\AA}^{-1}$ ) is somewhat smaller than in QSGW ( $k_F^\beta = 0.19\text{\AA}^{-1}$  and  $0.23\text{\AA}^{-1}$  in FeSe and FeTe, respectively).

For the 111-family, we show in Fig. 3 the Fermi surface of LiFeAs within QSGW, LDA and ARPES[10]. QSGW and ARPES agree very well for both large and small pockets: note in particular how QSGW shrinks the inner pockets at  $\Gamma$ . Both calculations and experiment[29] concur in the orbital characters along  $\bar{\Gamma X}$  : xy, yz, and xz, for the outer, middle and inner band, respectively. Within QSGW, the latter has moved below  $E_F$ . At  $M$  the smaller electron pocket is of mixed xz/yz; the bigger one, of xy character, is too small in LDA. It becomes larger in QSGW, as was previously found within LDA+DMFT[14, 30].

We turn to the mass enhancement relative to the LDA band masses, which have been used as a reference in the analysis of experiments. The enhancement is given as the ratio of the magnitude of the LDA and the QSGW group velocities near the Fermi level. The latter are

$$\frac{dE_{\mathbf{k}i}}{dk_\alpha} = \frac{\langle \Psi_{\mathbf{k}i} | \partial_{k_\alpha} (H^{\text{QSGW}} + \Re \Sigma^{\text{QSGW}}(\omega = 0)) | \Psi_{\mathbf{k}i} \rangle}{(1 - \langle \Psi_{\mathbf{k}i} | \partial_\omega \Re \Sigma^{\text{QSGW}} | \Psi_{\mathbf{k}i} \rangle)_{\omega=0}^{-1}} \quad (3)$$

A change in the velocity, and thus the effective mass, is possible through (a) the *dynamical* part of the self-energy via the quasi particle weight  $Z_k = 1/(1 - \partial_\omega \Re \Sigma^{\text{QSGW}}(k, \omega))_{\omega=0}$ . Noting that  $H^{\text{QSGW}} + \Sigma^{\text{QSGW}} = -\nabla^2 + v_{\text{crystal}} + v_{\text{Hartree}} - G^{\text{QSGW}}$  there is (b)

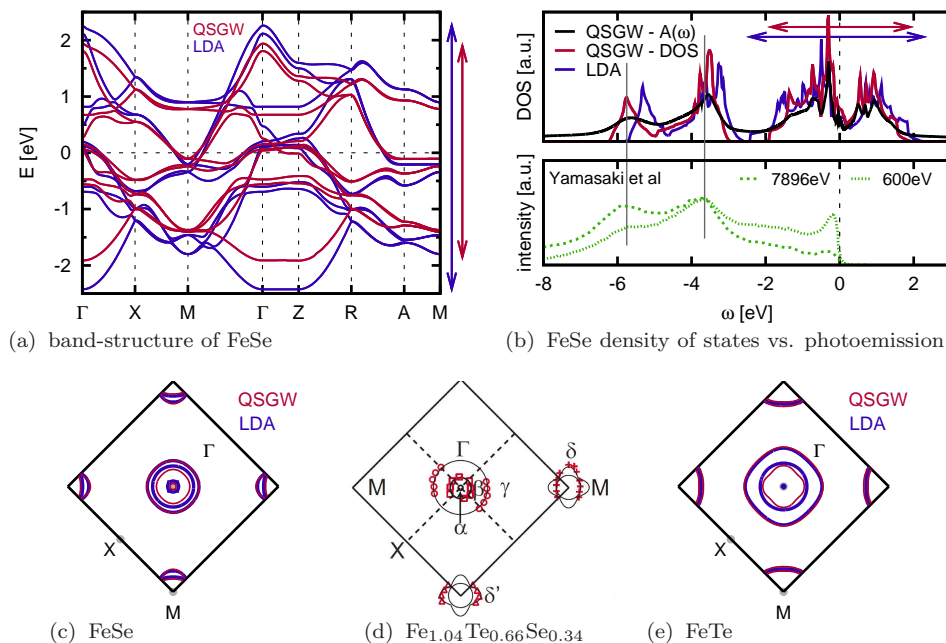


FIG. 2: **paramagnetic FeSe.** (a) band-structure within LDA and QSGW (notice the substantial bandwidth narrowing indicated by the arrows), (b) DOS in comparison to photoemission[11]. Also shown is the spectral function  $A(\omega)$  of the QSGW that takes into account lifetime effects. Arrows indicate the Fe-3d bandwidth; grey lines are guides to the eye. (c)-(e) Fermi surfaces : (c)/(e) FeSe/FeTe within QSGW and LDA, (d) experimental Fermi surface of  $\text{Fe}_{1.04}\text{Te}_{0.66}\text{Se}_{0.34}$  from ARPES[28].

	QSGW $\frac{m^{\text{QSGW}}}{m^{\text{LDA}}}$	QSGW $1/Z^{\text{QSGW}}$		ARPES $m^*/m^{\text{LDA}}$		DMFT $1/Z^{\text{DMFT}}$	
		xy	xz/yz	xy	xz/yz		
$\text{CaFe}_2\text{As}_2$	1.05	2.2	2.1	2.5[7]		2.7	2.0
$\text{SrFe}_2\text{As}_2$	1.13	2.3	2.0	3.0[8]		2.7	2.6
$\text{BaFe}_2\text{As}_2$	1.16	2.2	2.2	2.7 2.3 [9]		3.0	2.8
$\text{LiFeAs}$	1.15	2.4	2.1	3.0[10]		3.3/2.8	2.8/2.4
FeSe	1.22	2.4	2.2	3.6[11]		3.5/5.0	2.9/4.0
FeTe	1.17	2.6	2.3	6.9 [31]		7.2	4.8

TABLE I: **effective masses and quasi-particle weights.**  $m^{\text{QSGW}}/m^{\text{LDA}}$  denotes the ratio of the iron 3d bandwidth within QSGW and LDA. The quasi-particle weights  $Z^{\text{QSGW}}$  are extracted from  $\Sigma^{\text{QSGW}}$  at the  $\Gamma$  point in the band basis. DMFT masses from Ref. 14, except for the second values of LiFeAs (Ref. 30) and FeSe (Ref. 15). ARPES effective masses are obtained with respect to LDA, in accordance with Eq. (3).

a renormalization of the velocity through *non-local* correlations as encoded in  $G^{\text{QSGW}}$ , and (c) an effect through a change in charge density.

In DMFT approaches, the self-energy is local by construction, and enhanced masses emerge solely through the *energy dependence* of the self-energy (indeed  $m/m^{\text{DMFT}}=Z^{\text{DMFT}}$ ). While in many correlated materials, in which the physics is controlled by the on-site Coulomb interaction, there is evidence that this is a good approximation[32], it is not clear *a priori* whether such an ansatz is warranted for the pnictides and chalcogenides.

QSGW, on the other hand, accounts, albeit perturbatively, for all mechanisms of effective masses : Indeed, the momentum-dependence is manifestly included via Eq. (2), and the energy slope enters through the QSGW procedure, Eq. (1), that determines  $E_{\mathbf{k}}$ . By construction, Eq. (3) also reads  $\frac{dE_{\mathbf{k}i}}{dk_{\alpha}} = \langle \Psi_{\mathbf{k}i} | (\partial_{k_{\alpha}} H^{\text{QSGW}}) | \Psi_{\mathbf{k}i} \rangle$ , hence  $v_{xc}^{\text{QSGW}}$  accounts for, both, the dynamic and non-local renormalizations[45].

In order to discuss non-local and dynamic contributions to effective masses, we analyze the QSGW self-energy : Tab. I summarizes our results for the dynamical renormalization factors  $1/Z^{\text{QSGW}}$ , the net 3d bandwidth-narrowing,  $m^{\text{QSGW}}/m^{\text{LDA}}$ [46], as well as results from DMFT and ARPES. This reveals : (a) The inverse quasi-particle weights are larger than the actual bandwidth narrowing by a factor of two or more. One clear source of the discrepancy originates in the nonlocality of the self-energy, missing in both LDA and DMFT. Nonlocality tends to delocalize quasi-particles[33], see Eq. (3), which partially cancels the effects of the energy dependence of  $\Sigma$ . We analyze this further below. (b) The bandwidth narrowing  $m^{\text{QSGW}}/m^{\text{LDA}}$  is too small with respect to experiment. This is generally expected, since the reduction of the quasi-particle weight  $Z$  in correlated systems is a largely non-perturbative effect – a realm where DMFT excels. In particular, a DMFT study[14] rationalized that the large effective mass in FeTe is owing to the local Hund’s rule coupling, a multiplet effect not well treated in *GW*. Despite the insufficient dynamic renor-

malization, however, the trends in  $Z$  along the series of materials are captured, including the orbital differentiation. Indeed hole-like excitations of xy character are heavier than xz/yz ones for all compounds considered.

To make a direct connection with DMFT, we introduce a local basis set (indexed  $L$ ) by constructing maximally localized Wannier functions[34, 35] for the iron 3d and pnictogen/chalcogen 4p orbitals. We further introduce the momentum variance  $(\delta_k X)^2 = 1/N_L^2 \sum_{\mathbf{k}LL'} |\Re X_{LL'}^{\mathbf{k}} - \Re X_{LL'}^{loc}|^2$  of a quantity  $X$  with respect to its local reference  $X_{LL'}^{loc} = \sum_{\mathbf{k}} X_{LL'}^{\mathbf{k}}$ [47]. To quantify static corrections in QSGW beyond LDA at the Fermi level we define the many-body correction  $\tilde{\Sigma} = \Sigma^{QSGW} + H^{QSGW} - H^{LDA}$ , and compute its variance  $\delta_k \tilde{\Sigma}(\omega=0)$  [48]. We find  $\delta_k \tilde{\Sigma} = 0.08\text{eV}$  for  $\text{BaFe}_2\text{As}_2$ , and  $\delta_k \tilde{\Sigma} = 0.09\text{eV}$  for FeSe, while the variations of the LDA exchange-correlation potential,  $\delta_k v_{xc}^{LDA}$ , are 0.22eV and 0.2eV, respectively. Hence, QSGW overall reduces the momentum dependence, consistent with the observed bandwidth-narrowing, see Eq. (3). The relative change in the momentum variation,  $\delta_k \tilde{\Sigma} / \delta_k v_{xc}^{LDA}$ , is important in both compounds : 36% for  $\text{BaFe}_2\text{As}_2$  and 45% in FeSe. This shows that the assumption of a purely local self-energy correction (à la DMFT) is not fully warranted.

To quantify the momentum dependence of the quasi-particle dynamics, we introduce the variance  $\Delta_k Z = \sqrt{\sum_{\mathbf{k}L} |Z_{LL}^{\mathbf{k}} - Z_{LL}^{loc}|^2}$  of the Fermi liquid weight. We find  $\Delta_k Z \approx 0.5\%$  for all  $GW$  calculations performed here[49]. This establishes that non-local and dynamical correlation effects are essentially *separable*. Thus the self-energy is describable by the ansatz  $\tilde{\Sigma}(\mathbf{k}, \omega) = F(\mathbf{k}) + (1 - Z^{-1})\omega$  within the Fermi liquid regime, which encompasses (within QSGW) the range  $|\omega| \lesssim 2\text{eV}$ . The QSGW self-consistency further imposes :  $F(\mathbf{k}) = Z^{-1}E_{\mathbf{k}} - \epsilon_{\mathbf{k}}^{LDA}$ .

To introduce non-local correlations to DMFT, or,

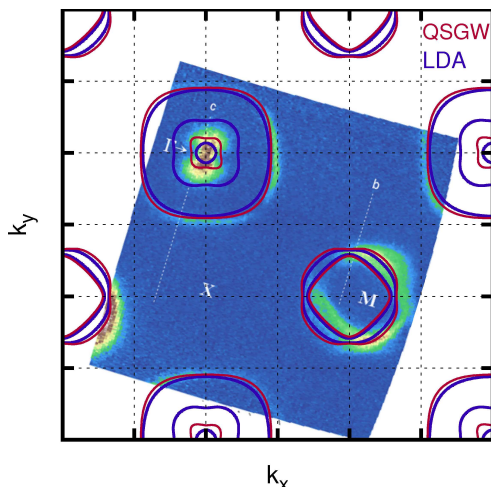


FIG. 3: **Fermi surface of LiFeAs.**  $k_z = 0$ -plane in the Brillouin zone for 2 Fe atoms; experimental intensity from Ref. 10. Notice how QSGW drastically shrinks the inner pockets at  $\Gamma$ .

reversely, to improve on local fluctuations in  $GW$ , a  $GW$ +DMFT scheme has been proposed[36]. In the simplest of implementations local and non-local self-energies from DMFT and  $GW$ , respectively, are combined. This was rationalized further by noting that self-energy contributions *beyond*  $GW$  are mostly local[37], thus amenable to DMFT. Here, we showed that *even on the  $GW$  level*, the (low-energy) dynamics is essentially local, too. Hence, non-local correlations can be accounted for by the *static* QSGW potential. This has several advantages : Due to its complexity,  $GW$ +DMFT has, so far, only been employed non-selfconsistently[36, 38]. This defies many of the method’s virtues, e.g. it persists a starting point dependence, and issues of double counting. Here, we advocate to circumvent this by imposing (quasi-particle) self-consistency for the  $GW$  only, i.e. introducing a QSGW+DMFT scheme. The latter is manifestly void of any DFT dependence, and the double counting is well defined [50].

For the iron pnictides and chalcogenides we conclude that the QSGW approach yields very good Fermi surfaces, as well as sizable corrections to spectral features at finite energies. We further showed that non-local correlations are important, and can be incorporated through the QSGW effective potential. Moreover we showed that dynamical correlations are mostly local. They are not sufficiently accounted for in QSGW, especially when correlations are strong, as in the chalcogenides. These findings suggest that QSGW and DMFT taken together will be sufficient to incorporate most of the correlations in electronic structure.

The support of the DOE-CMSN grant “Computational Design of Fe Based Superconductors” is gratefully acknowledged.

- 
- [1] J. Paglione and R. L. Greene, Nat Phys **6**, 645 (2010).
  - [2] S. Lebegue, Phys. Rev. B **75**, 035110 (2007).
  - [3] D. J. Singh and M.-H. Du, Phys. Rev. Lett. **100**, 237003 (2008).
  - [4] J. Dong, H. J. Zhang, G. Xu, et al., Europhysics Letters **83**, 27006 (2008).
  - [5] M. M. Qazilbash, J. J. Hamlin, R. E. Baumbach, et al., Nat. Phys **5**, 647 (2009).
  - [6] T. Terashima, M. Kimata, N. Kurita, et al., Journal of the Physical Society of Japan **79**, 053702 (2010).
  - [7] Q. Wang, Z. Sun, E. Rotenberg, et al., ArXiv:1009.0271 (2010).
  - [8] M. Yi, D. H. Lu, J. G. Analytis, et al., Phys. Rev. B **80**, 174510 (2009).
  - [9] V. Brouet, M. Fuglsang Jensen, A. Nicolaou, et al., ArXiv:1105.5604 (2011).
  - [10] S. V. Borisenko, V. B. Zabolotnyy, D. V. Evtushinsky, et al., Phys. Rev. Lett. **105**, 067002 (2010).
  - [11] A. Yamasaki, Y. Matsui, S. Imada, et al., Phys. Rev. B **82**, 184511 (2010).
  - [12] Q. Huang, Y. Qiu, W. Bao, et al., Phys. Rev. Lett. **101**,



- 257003 (2008).
- [13] H.-F. Li, W. Tian, J.-Q. Yan, et al., Phys. Rev. B **82**, 064409 (2010).
- [14] Z. P. Yin, K. Haule, and G. Kotliar, Nat. Mat **10**, 932 (2011).
- [15] M. Aichhorn, S. Biermann, T. Miyake, et al., Phys. Rev. B **82**, 064504 (2010).
- [16] M. Aichhorn, L. Pourovskii, and A. Georges, Phys. Rev. B **84**, 054529 (2011).
- [17] G. Wang, Y. Qian, G. Xu, et al., Phys. Rev. Lett. **104**, 047002 (2010).
- [18] F. Aryasetiawan, J. M. Tomczak, T. Miyake, et al., Phys. Rev. Lett. **102**, 176402 (2009).
- [19] S. V. Faleev, M. van Schilfgaarde, and T. Kotani, Phys. Rev. Lett. **93**, 126406 (2004).
- [20] M. van Schilfgaarde, T. Kotani, and S. Faleev, Phys. Rev. Lett. **96**, 226402 (2006).
- [21] T. Kotani, M. van Schilfgaarde, and S. V. Faleev, Phys. Rev. B **76**, 165106 (2007).
- [22] G. Kotliar, S. Y. Savrasov, K. Haule, et al., Rev. Mod. Phys. **78**, 865 (2006).
- [23] Y. Zhang, F. Chen, C. He, et al., Phys. Rev. B **83**, 054510 (2011).
- [24] S. Thirupathaiah, S. de Jong, R. Ovsyannikov, et al., Phys. Rev. B **81**, 104512 (2010).
- [25] T. Suda, Y. Wakasaka, T. Mizokawa, et al., Journal of the Physical Society of Japan **80**, 113707 (2011).
- [26] B. Mansart, V. Brouet, E. Papalazarou, et al., Phys. Rev. B **83**, 064516 (2011).
- [27] J. Fink, S. Thirupathaiah, R. Ovsyannikov, et al., Phys. Rev. B **79**, 155118 (2009).
- [28] F. Chen, B. Zhou, Y. Zhang, et al., Phys. Rev. B **81**, 014526 (2010).
- [29] T. Hajiri, T. Ito, R. Niwa, et al., Phys. Rev. B **85**, 094509 (2012).
- [30] J. Ferber, K. Foyevtsova, R. Valentí, et al., Phys. Rev. B **85**, 094505 (2012).
- [31] A. Tamai, A. Y. Ganin, E. Rozbicki, et al., Phys. Rev. Lett. **104**, 097002 (2010).
- [32] G. Kotliar and D. Vollhardt, Physics Today **57**, 53 (2004).
- [33] R. Asgari, B. Davoudi, M. Polini, et al., Phys. Rev. B **71**, 045323 (2005).
- [34] N. Marzari and D. Vanderbilt, Phys. Rev. B **56**, 12847 (1997).
- [35] T. Miyake and F. Aryasetiawan, Phys. Rev. B **77**, 085122 (2008).
- [36] S. Biermann, F. Aryasetiawan, and A. Georges, Phys. Rev. Lett. **90**, 086402 (2003).
- [37] N. E. Zein, S. Y. Savrasov, and G. Kotliar, Phys. Rev. Lett. **96**, 226403 (2006).
- [38] J. M. Tomczak, M. Casula, T. Miyake, et al., submitted (2012).
- [39] M. Methfessel, M. van Schilfgaarde, and R. Casali, in Electronic Structure and Physical Properties of Solids: The Uses of the LMTO Method, Lecture Notes in Physics. H. Dreysse, ed. **535**, 114 (2000).
- [40] T. Miyake, K. Nakamura, R. Arita, et al., Journal of the Physical Society of Japan **79**, 044705 (2010).
- [41] J. M. Tomczak, F. Aryasetiawan, and S. Biermann, Phys. Rev. B **78**, 115103 (2008).
- [42] A matrix structure in the space of orbitals is assumed.
- [43] Our LDA results (method of Ref. 39) are congruent with previous works, e.g. Ref. 40.
- [44] Interestingly, the spin-orbit coupling makes a qualitative difference here. Indeed without it, the pockets are reversed in LDA, thus yielding wrong orbital characters.
- [45] For insulating  $\text{VO}_2$  correlation effects from a DMFT cluster extension were found to be mappable onto a non-local one-particle potential[41] akin to the  $\text{QS}GW$  procedure.
- [46] We find the ratio of bandwidths is very similar to the inverse ratio of group velocities on the Fermi surface.
- [47] We restrict  $L, L'$  to the 3d orbitals of iron.
- [48] The Wannier functions based on the LDA and the  $\text{QS}GW$  are of course different. However, as the Wannier spread differ by less than 3%, we neglect this effect.
- [49]  $\Delta_k [1 - \partial_\omega \Re \Sigma^{\text{QS}GW}(k, \omega)]^{-1} < Z/10$  for  $|\omega| < 2\text{eV}$ : the momentum variance of the quasi-particle dynamics is small.
- [50] namely by the local projection of  $G^{\text{QS}GW}$ .